X-693-84-9



# ACOUSTO-OPTIC SPECTROMETER I. NOISE CONTRIBUTIONS AND SYSTEM CONSIDERATION


Author GORDON CHIN
Code 693.1

APRIL 1984

NASA
National Aeronautics and Space Administration

GODDARD SPACE FLIGHT CENTER
GREENBELT, MARYLAND

# Acousto-Optic Spectrometer (AOS) as a Radiometer

## I. Noise Contributions and System Considerations

Gordon Chin

NASA/Goddard Space Flight Center
Laboratory for Extraterrestrial Physics
Code 693.1
Infrared and Radio Astronomy Branch
Greenbelt, MD 20771

ABSTRACT

An Acousto-Optic Spectrometer (AOS) used as an IF spectrometer to a heterodyne receiver is modeled as a total power multi-channel integrating receiver. Systematic noise contributions common to all total power, time integrating receivers as well as noise terms unique to the use of optical elements and photo-detectors in an AOS are identified and discussed. In addition, degradation of signal-to-noise ratio of an unbalanced Dicke receiver compared to a balanced Dicke receiver is found to be due to gain calibration processing and is not an instrumental effect.

Key Words: Acousto-optics, Bragg cell, IF spectrometer

## FOREWORD

The advantages of using acousto-optic techniques as IF spectrometers come from the simplicity of a small number of discrete components necessary to construct a system. This simplicity gives rise to compactness, low power requirements, and low weight which is even more important as heterodyne receivers are pushed into frequency ranges where remote platforms are necessary to minimize signal attenuation from the earth's atmosphere. In addition, the use of waveguide and integrated-optic components offers an additional degree of miniaturization which can further simplify alignment and ruggedization problems of remote IF spectrometers.

In this report we will enumerate possible sources of noise which will be associated with the use of acousto-optic techniques as total power radiometers. Some noise sources are common to all multi-channel power radiometers while other noise sources are unique to the use of optical components and photodetectors as essential elements of the radiometric system. We will see that additional signal to noise improvement can be achieved by digital processing over analog integration on the photodetectors. However, the use of analog to digital converters, ADCs, requires careful consideration of the linearity of the data conversion to insure that one can obtain the necessary sensitivity to small signals required for astronomical observations. In addition, we derive a degradation in the signal to noise ratio that occurs when instrumental calibration is taken into account in an unbalanced Dicke-switched system.

Noise source measurements in both bulk and integrated optics AOS's will be presented in a future report. This study will form the basis of a systematic comparison between actual devices.

# I. INTRODUCTION

Whether we use bulk or integrated-optics techniques, an acousto-optic spectrometer (AOS) is composed of four main components; laser light source, collimating and focusing optics, acoustic transducer, and detector array. The principle of operation remains the same for both types of system. A conceptual diagram of an AOS is shown in Fig. 1. An ultrasonic delay line is used to convert wide-band RF input to a proportional spatial pattern by means of a traveling pressure wave in a crystal. The spatial variation created in the index of refraction of the crystal is used to modulate coherent light, and the diffracted spectral components are separated by a lens. The Fourier transform of the RF input signal is distributed on the output plane of the lens, and the light intensity is detected by an array of photodiodes, yielding the instantaneous power spectrum of the RF input signal.

Specifically, a given RF signal, g(t), can be decomposed by the Fourier transform relationship into plane wave components (cf. [1]).

$$g(t) = \int G(f)e^{-i2\pi tf}df \qquad (1)$$

where G(f)df can be interpreted as the amplitude of a plane wave of frequency f launched by an ultrasonic transducer into a crystal, or onto a substrate surface by a SAW transducer as in an integrated-optics AOS.

The interaction of this wave train (equation 1) with the optical beam results in a superposition of plane-wave deflected beams provided that the Bragg condition is satisfied for each component, i.e. $\sin\alpha_B = \lambda/2\Lambda$ where $\lambda$ is the wavelength of light, and $\Lambda$ is the acoustic wavelength.

Often it is necessary to design a set of phased transducers to achieve

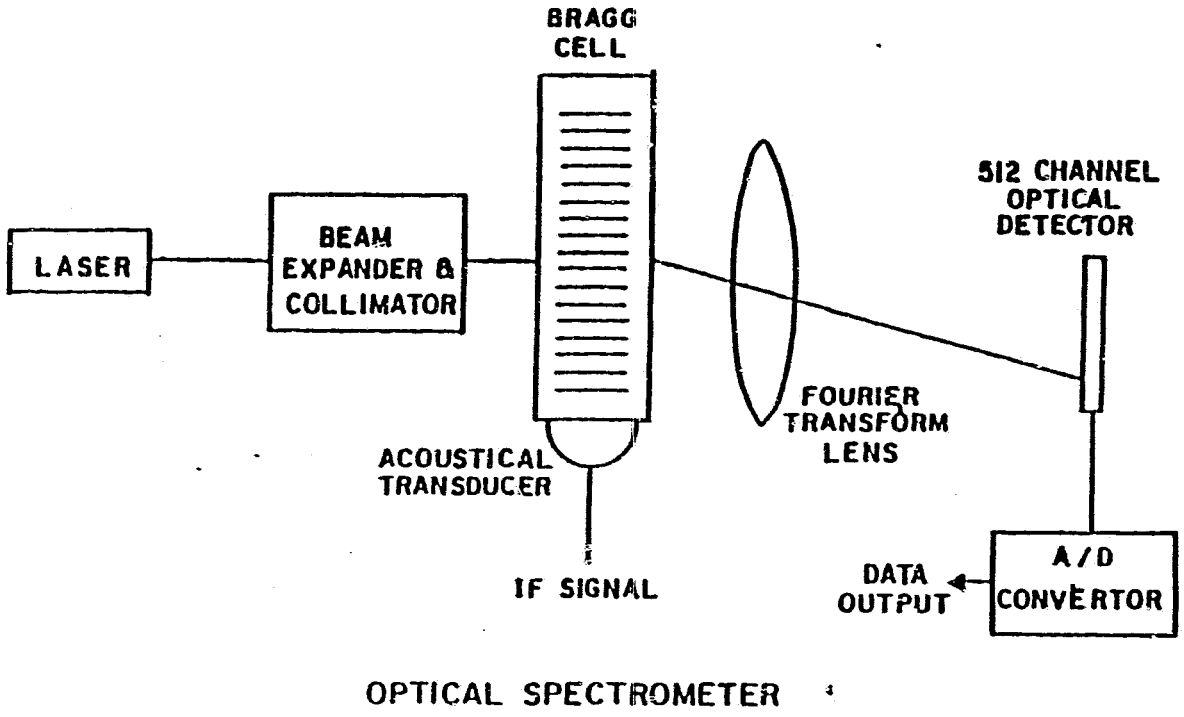


FIGURE 1. Schematic diagram of components of an Acousto-Optic Spectrometer.

wideband RF response since it is impossible for a single transducer to meet the Bragg condition for all input frequencies. The propagating acoustic wave can be described by replacing t with $t_o$

$$g(t) = \int e^{-i2\pi t_o f} G(f) e^{(2\pi f/v)z} df \qquad (2)$$

where $t_o$ is the reference time (given by time of excitation), v is the acoustic velocity, and z is the coordinate aligned with the direction of the acoustic wave vector.

The deflected optical beam generated in a Bragg cell modulator is proportional to the product of the incident beam wavefront $E_i(z)$, the acoustic wavefront g(t), and the efficiency of the interaction $\eta(f)$. A fraction of the light acquires a new direction of propagation as a result of the interaction, with the angle of deflection given by $\theta=\lambda f/v$ (see Fig. 2).

The deflected beam $E_d(z)$ emerging from the acousto-optic interaction is given by

$$E_d(z) = \int E_i(z) G(f) \eta(f) e^{i(2\pi f/v)z} df \qquad (3)$$

In coherent illumination, a lens of focal length F will give at its back focal plane a field distribution which is the Fourier transform of the field distribution in its front focal plane; i.e.

$$E_2(y) = C \int E_d(\bar{z})\ e^{i(2\pi/\lambda F)yz} d\bar{z} \qquad (4)$$

where C is a constant, and y is the transverse coordinate axis in the back focal plane. If $E_d(\bar{z})$ is not in the front focal plane, the output distribution $|E_2(y)|^2$ is not changed, but a constant phase factor $e^{ix(y)}$ is added to equation

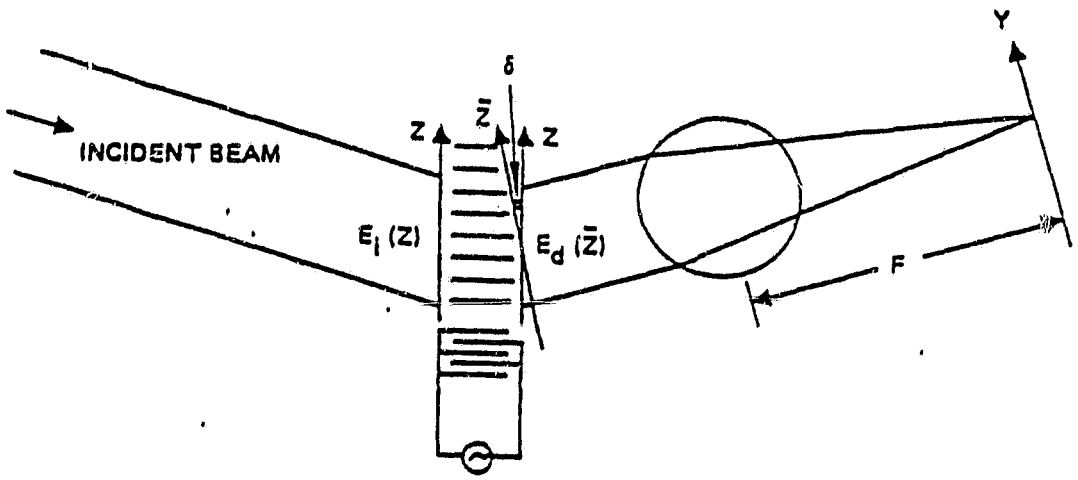


FIGURE 2. Optical wavefront propagation through the acoustooptic interaction region and the transform lens.

(4) that is not detectable in power measurements.

Combining equations (3) and (4), and substituting with $\bar{z}\cos\delta$ to account for the new propagation direction gives the field distribution at the detector plane

$$E_2(y)=C\int\int G(f)\eta(f)w(\bar{z})e^{i2\pi(\bar{z}\cos\delta/v)f}\,e^{i(2\pi/\lambda f)y\bar{z}}\,df\,d\bar{z} \qquad (5)$$

where $w(\bar{z})$ is a weighting function determined by the optical aperture size, incident optical wavefront distribution, and system aberration. For example, a Gaussian laser beam and an aberration-free system will yield a truncated Gaussian form for $w(\bar{z})$.

Carrying out the integration over $\bar{z}$ in equation (5), and denoting W as the Fourier transform of $w(\bar{z})$ gives

$$E_2(y)=C\int G(f)\eta(f)W(y+F\lambda\cos\delta/v)df \qquad (6)$$

with $y+(F\lambda\cos\delta/v)$ the argument for W.

We see from equation (6) that the output intensity distribution $|E_2(y)|^2$ is positioned linearly in proportion to the frequency of the modulating signal and its intensity is proportional to the strength of the spectral component at frequency f multiplied by the efficiency of the Bragg modulator. A well designed optical spectrum analyzer should have frequency as well as intensity linearity.

The intensity of the diffracted light in the Bragg region is given by [2]

$$\frac{I_1}{I_0}=\eta\,\mathrm{sinc}^2\left(\pi+\left(\frac{\Delta k\,L}{2}\right)^2\right)^{1/2} \qquad (7)$$

where $I_1$, and $I_o$ represent the diffracted and incident light intensity, $\Delta k$ the momentum mismatch between the incident light and acoustic propagation vectors, and L is the interaction length of the acoustic wave column

$$\eta = \frac{\pi^2}{2\lambda^2} \left( \frac{n^6 p^2}{\rho v^3} \right) \frac{1}{H} P_a \qquad (8)$$

where p is the photoelastic coefficient, $\rho$ is the mass density, v is the acoustic velocity, H is the height of the acoustic beam, $P_a$ is the acoustic power, and the quantity $n^6p^2/\rho v^3$ is the acoustic figure of merit $M_2$. In the small argument limit equation (7) yields

$$\frac{I_1}{I_o} = \eta \qquad (9)$$

so that $\eta$ gives directly the diffraction efficiency of the device.

For an acoustic modulator with RF bandwidth $\Delta f$, the total angular deflection $\Delta\delta = \Delta f\ \lambda/v$, the number of resolvable angles N is determined by the total angular deflection divided by the resolvable angular spread, $\lambda/L$, of the light beam.

$$N = \frac{\Delta\delta}{\lambda/L} = \frac{\lambda \Delta f}{v} \cdot \frac{L}{\lambda} = \Delta f \frac{L}{v} = \tau \Delta f \qquad (10)$$

where $L/v = \tau$ is the aperture, i.e. the time of interaction between the acoustic wave and light. N is called the time-bandwidth product of a particular Bragg modulator. [3]

## II. Total Power Time Integrating Radiometer

An AOS can be regarded as a total power, multichannel radiometer with each channel modeled as shown in Fig. 3 by a square law detector, with a passband

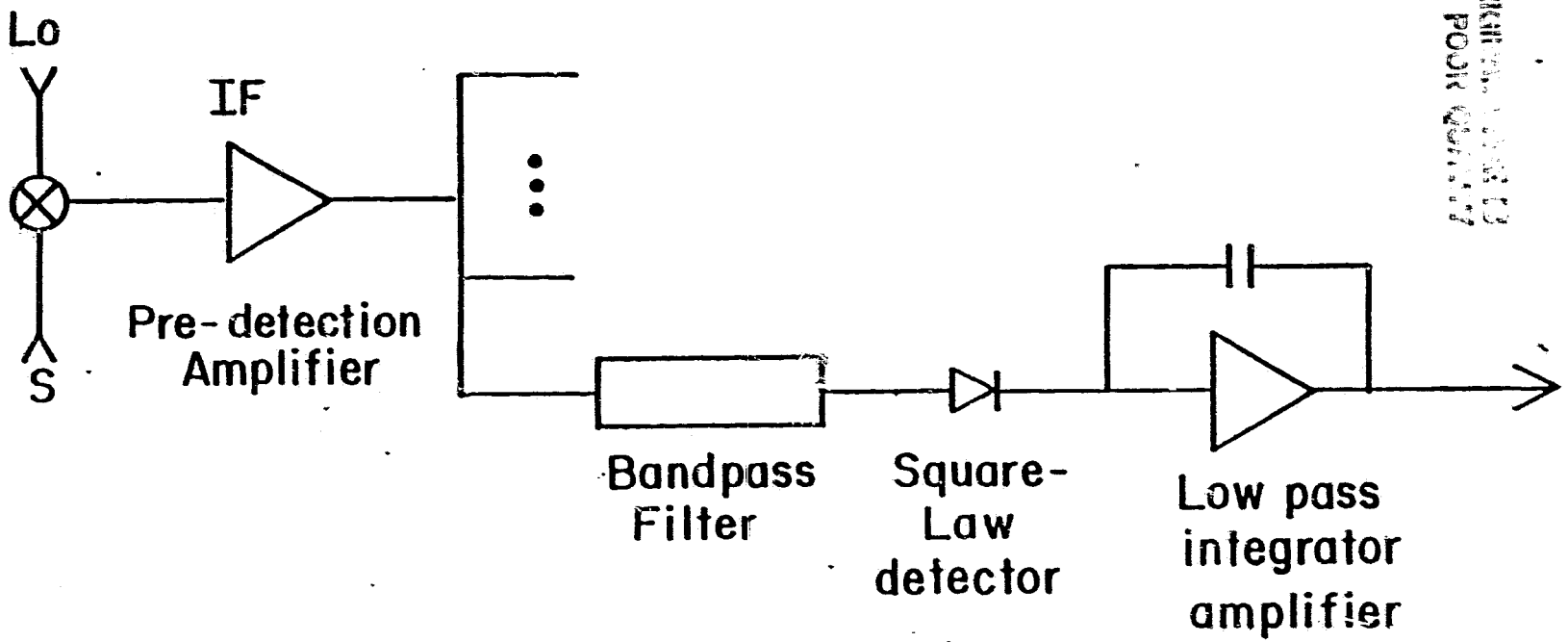


FIGURE-3. Schematic diagram of a multi-channel total power time integrating radiometer.

filter of bandwidth B, and an integrator with time constant T. The advantage of such a system comes from a processing gain in signal to noise which derives from the analog time integration (cf. Kraus [4], Lucas [5], Kellman et al. [6], and a short discussion in Turpin [7]). Specifically, if the input to the square law detector is a Gaussian zero mean signal and is assumed to be band limited by the pre-detection amplifier section, then the filtered voltage, $V_{IF}$, resembles a randomly modulated carrier wave at the IF frequency. The amplitude distribution of the wave form has a Rayleigh distribution given by (see discussion in Kraus [4]),

$$P(v) = \frac{v}{V_{eff}} e^{-(v^2/2V^2_{eff})} \tag{11}$$

The statistical properties of equation (11) can be found in Whalen [8] and are given by

$$\mu = \sigma = V_{eff} \tag{12}$$

that is the mean voltage of equation (11) is equal to the rms standard deviation, $\sigma$, of the Rayleigh distribution. The output of the integrator can be viewed as taking N = BT independent samples of the diode output and after an integration time T the integrator output is given by

$$V_{out} = BT\,\mu \tag{13}$$

while the rms standard deviation of the output voltage is given by

$$\sigma_{out} = \sqrt{BT}\ \sigma \tag{14}$$

We see that the output of the integrator, therefore, will be a DC voltage level effectively determined by the system noise. If a small signal component is present in addition to the Gaussian noise, the band-limited probability distribution in equation (11) evolves to a series of distribution curves called Rician density functions (Whalen [8]), with the functions approaching a Gaussian distribution for higher input signal to noise ratio.

The integrator output with a signal present is given by

$$V_S = BTS \tag{15}$$

where S is the signal power. Since we are only interested in the signal contribution, we subtract off the DC bias of the noise output to derive the signal to noise ratio,

$$SNR_{out} = \frac{\Delta V_{out}}{\sigma_{out}} = \frac{BT}{\sqrt{BT}} \frac{S}{\sigma} = \sqrt{BT}\ SNR_{in} \tag{16}$$

By integration we obtain an improvement in signal to noise ratio given by $\sqrt{BT}$, which is called the analog processor gain.

Further sensitivity improvements can be achieved by digital integration with extended precision. We digitize the integrator output with an analog to digital converter (ADC) after the analog integration period T. With J integration periods the digital sum is given by the mean value

$$\mu_{digital} = J\ V_{out} = J\mu BT$$

$$\Delta\mu_{digital} = J\ \Delta V_{out} = J\ S\ BT \tag{17}$$

The variance on the digitized mean is given by

$$\sigma_{digital} = \sqrt{JBT}\ \sigma \tag{18}$$

The SNR improvement using digital processing is given by

$$SNR_{digital} = \sqrt{J}\ SNR_{out} = \sqrt{JBT}\ SNR_{in}, \tag{19}$$

and, therefore, we gain a factor $\sqrt{J}$ improvement in signal to noise ratio over the analog process; this gain is only limited by digital precision.

## III. Degradations in Signal to Noise Ratio from Ideal

In the calculations of analog and digital processing gains, numerous additional sources of noise have been neglected which degrades the ideal SNR given by equation (19). Among the factors which degrade receiver performance and are common to all square-law detector systems are the following:

a. Receiver Fluctuations

The total system noise is determined primary by the mixer and IF pre-amplifier noise figure. Additional stages of gain, especially in a room-temperature astronomical heterodyne system which may encompass as much as 90 dB of amplification, contribute negligibly to the system noise performance. This relationship is shown by

$$T_{sys} = T_1 + \frac{T_2}{G_2} + \frac{T_3}{G_2 G_3} + \cdots \tag{20}$$

where $T_1$ is determined by the mixer noise temperature and conversion losses, $T_2$

is the noise temperature of the first amplifier with gain given by $G_2$, and further stages of amplification is represented by a noise temperature $T_3$, and gain $G_3$. Fluctuations in local oscillator power or in mixing efficiencies contribute directly to the system temperature. Heterodyne receivers employing laser local oscillators and photoconductor mixing elements are particularly vulnerable to this type of fluctuation since mixing efficiency and system noise depend critically on laser power stability and optical alignment. If the first stage of amplification has particularly high gain and is dominated by $T_1$, amplifier stability will also be critical for high sensitivity.

Receiver fluctuations alter the sensitivity by adding a post-detection noise term to equation (14), and is given by

$$\sigma^2_{out} = BT\sigma^2_{RF} + (\Delta F)^2 \sigma^2_{RF} \tag{21}$$

where we denote $\sigma_{RF}\ \Delta F$ as the noise contribution from receiver fluctuations, and $\Delta F$ is the scale of fluctuations with respect to $\sigma_{RF}$. If the receiver fluctuations are confined to low frequencies, this is true for amplifiers and regulated power supplies, then fluctuation noise can be reduced by synchronous detection. In Dicke switching [9], the signal is modulated in a square wave fashion against a load, with the modulation frequency chosen to be higher than fluctuation frequencies. The signal is recovered by multiplying the detector output by a square wave which effectively removes the DC level. However, Dicke switching reduces the signal integration time by two, and therefore halves the processing gain given by equation (16). The degraded signal to noise ratio offered by Dicke switching is given by

$$SNR_{out} = \frac{BT}{2\sqrt{BT+(\Delta F')^2}}\ SNR_{in} \tag{22}$$

where $\Delta F'$ is receiver fluctuation noise reduced by Dicke switching.

Since almost all astronomical receivers use Dicke switching we will use

equation (22) for our standard SNR.

b. Analog to Digital Converter Noise

The penalty in increasing SNR gain via digital processing is the introduction of quantization noise from the finite resolution of an analog to digital converter (ADC). In using an ADC, care must be taken to insure that the intrinsic noise, $\sigma_{RF}$, is equal to or greater than the quantization step, $\Delta$, i.e.

$$\Delta = K\sigma_{RF} \quad , \quad K < 1 \tag{23}$$

If equation (23) is satisfied, then a digitization sample can be modeled to have the following statistical properties. An ADC will put out a number proportional to the input voltage given by the transfer function shown in Fig. 4. This assumes that the ADC has uniform step sizes and therefore is an ideal step size quantifier. The output can be written as

$$V_o = V_i + e \tag{24}$$

where e is the error between the ADC outputted code and the true voltage value. If equation (23) holds, we can represent the probability distribution of e as

$$p(e) = (1/\Delta) \qquad \text{for} \quad -\Delta/2 \leq e \leq \Delta/2 \tag{25}$$

Equation (25) implies that the errors are randomly distributed over the quantization interval. The mean is given by

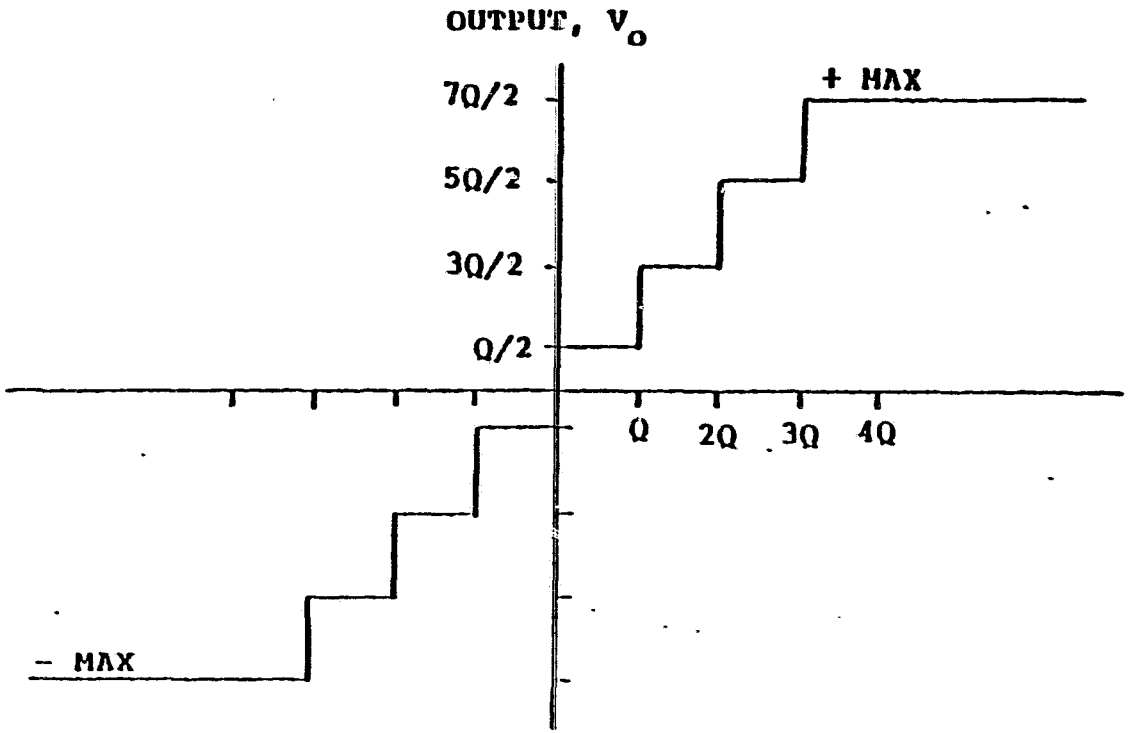


FIGURE 4. Ideal digital transfer function for 3-bit ADC.

$$\mu_e = \int_{-\Delta/2}^{+\Delta/2} (1/\Delta)\, e \; de = 0 \qquad (26)$$

while the standard deviation is given

$$\sigma_e^2 = \int_{-\Delta/2}^{+\Delta/2} p(e)(e-\mu_e)^2 de = (1/\Delta) \int_{-\Delta/2}^{+\Delta/2} e^2 \, de$$

$$= (1/\Delta)\, e^3/3 \;\Big|_{-\Delta/2}^{+\Delta/2} = \Delta^2/12 = K^2 \sigma_{RF}^2/12 \qquad (27)$$

Equation (26) guarantees that after averaging enough ADC samples we get the true average value, i.e. since $\mu_e = 0$

$$\bar{V}_{out} = E\{ V_o \} = E\{ V_i + e \} = E\{ V_i \} + \mu_e = \bar{V} \qquad (28)$$

It is easy to show that for every additional bit of resolution in an ADC, the SNR improves by 6 dB. Since the error distribution is uncorrelated, the error power spectrum will be that of white noise.

Equation (19) and (22) can now be modified to include the effects of quantization noise.

$$SNR_{digit} = \frac{BT\sqrt{J}}{2} \frac{SNR_{in}}{\sqrt{BT + (\Delta F')^2 + K^2/12}} \qquad (29)$$

and the degradation in the SNR is therefore given by

$$\delta = \sqrt{1 + (\Delta F')^2/BT + K^2/12BT} \qquad (30)$$

To insure that receiver fluctuations and quantization noise do not degrade the receiver performance, requires that

$$BT \gg (\Delta F')^2 \quad \text{and}$$
$$BT \geq K^2/12 \qquad (31)$$

The proper use of an ADC requires that $K \leq 1$; if $K = 1$ (i.e. the quantization step size is equal to the noise), the requirement that $BT \geq 1/12$ in equation (31) is easy to meet since BT is usually much greater than 1. Therefore ADC quantization noise degrades the SNR negligibly under proper operating conditions.

c. Differential Linearity

In heterodyne receivers where the aim is to recover a small signal out of a receiver with large noise, it is important that errors in differential linearity of the system be as small as possible. The major source of differential non-linearity comes from the use of ADCs. These errors, however, can be minimized by proper selection of the converters. In Fig. 5, the widths of three different ADCs are plotted for 256 consecutive digital codes. Although the manufacturer's published specifications for all three converters stated ± 1/2 LSB differential linearity, this performance was satisfied in only one of the

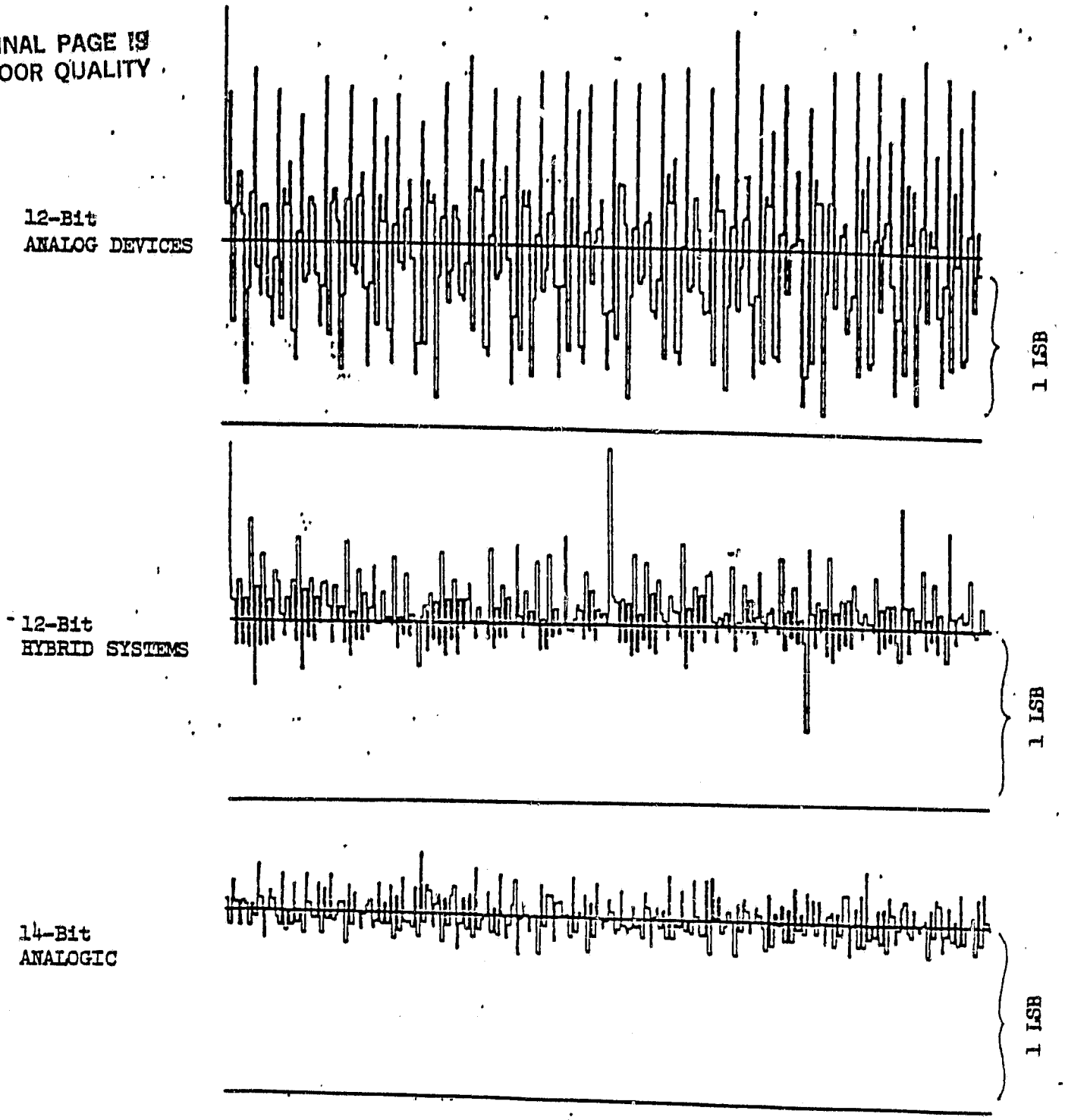


FIGURE 5. Histogram of ADC code_widths with respect to 1 LSB.

three ADCs tested. The results given in Fig. 5 are consistent with the tests of the same model for other units by the same manufacturer. We can see that the worse case is that of the 12-bit Analog Devices ADC whose differential error is about ± 0.75 LSB, whereas the best case is the 14-bit Analogic ADC whose differential error is ± 0.1 LSB. In the Hybrid Systems ADC the average error is about ±0.25 LSB but with excursions of + 1, - 1/2 LSB in this voltage range.

Differential non-linearities affect our measurements by altering the incremental linearity or the digital transfer function from an ideal one. The transfer function of a particularly bad ADC is illustrated in Fig. 6 in contrast to an ideal incremental transfer function shown in Fig. 4. The bit sizes, $\Delta_i$, in Fig. 6 are all different as compared to the uniform step sizes given by an ideal ADC in Fig. 4. In an observation, the actual transfer function is convolved with a Gaussian of width $\sigma_{RF}$ which is represented in Fig. 6 by the smooth curve; however, the convolved digital transfer function will depart from the ideal one given by the unit slope dotted line.

In detecting a small signal by means of subtracting a large DC offset representing the receiver noise, the absolute error in the digital transfer function is not the determining factor which gives the error in the measurement, rather it is the departure from unity of the slope of the transfer function at the reference operating point, i.e. since

$$\Delta S = m(V)\Delta V_{in} \tag{32}$$

where m is slope at the reference voltage, V, and $\Delta V$ is the signal difference. The error in the measurement can then be given by

$$\epsilon(V) = \Delta m \cdot (V)\ \Delta V \tag{33}$$

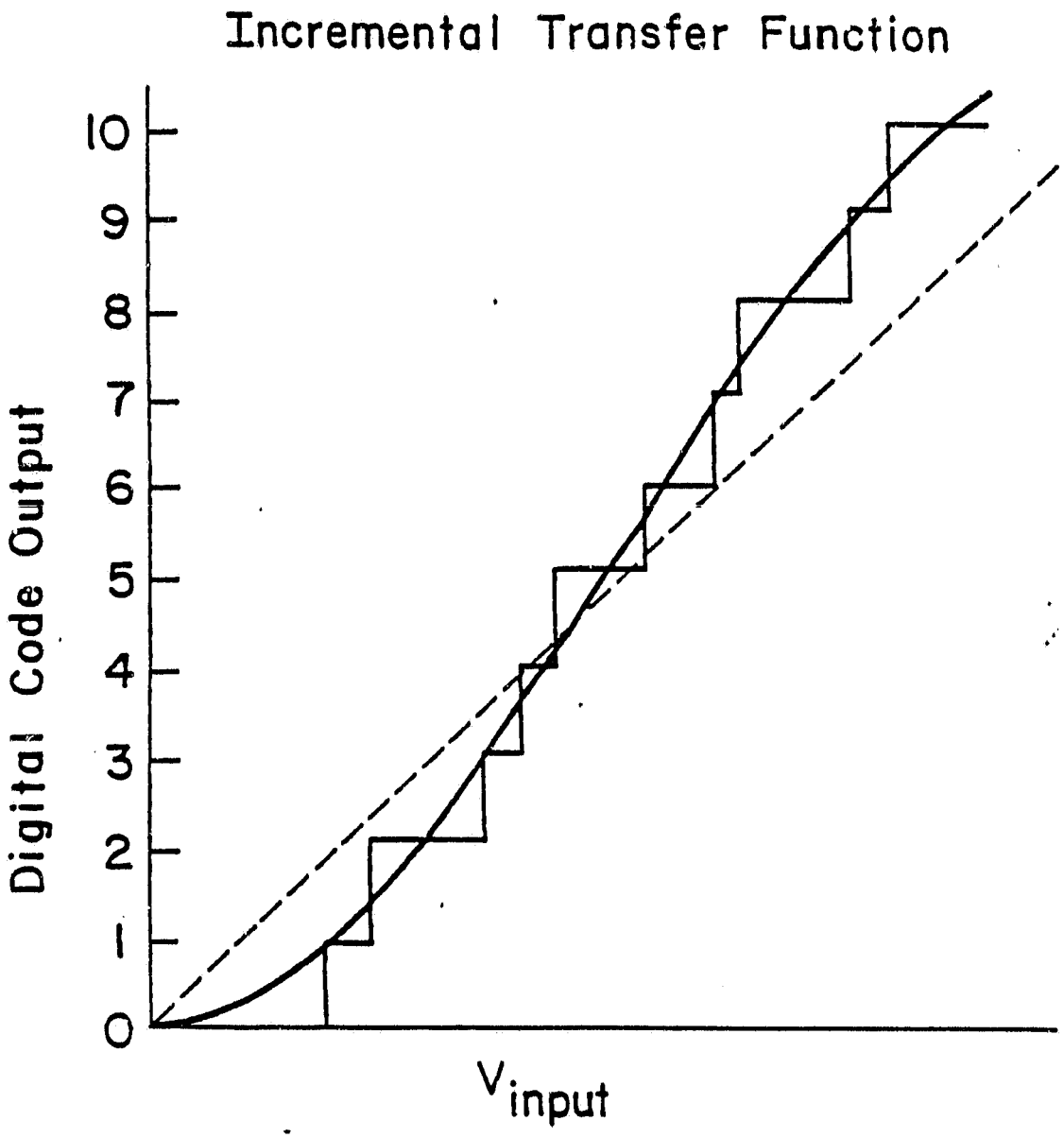


FIGURE 6. Non-ideal ADC incremental transfer function. Solid line represents convolved non-linear transfer function compared to ideal ( dotted line).

where $\varepsilon(V)$ is the error function of the reference voltage, $\Delta m(V)$ is the deviation from unity of the slope of the digital transfer function, i.e. $m(V) = 1 + \Delta m(V)$.

Since the error is a function of V, the errors of independent measurements of $\Delta S$ can no longer be uncorrelated. This is due to the fact that in deriving the smoothed digital transfer function, we convolved the incremental transfer function with a Gaussian of width $\sigma$, which defined the deviation we can expect from V. Therefore $\Delta m(V)$ will be, on the average, the slope error we can expect at the reference voltage. We then see that $\varepsilon(V)$ will be the limiting sensitivity since we cannot integrate to a value below $\varepsilon(V)$, defined by the differential non-linearity error. In the previous sections we saw that with N observations of a signal, the signal increased as N, i.e. $S = N\Delta S$, while the uncorrelated noise increase as $\sqrt{N}$, i.e. $\sigma_s^2 = \Sigma\, \sigma^2 = N\sigma^2$, therefore $\sigma_s = \sqrt{N}\sigma$. and the $SNR_{out} = s/\sigma_s = \sqrt{N}\, SNR_{in}$. However, with correlated noise, the noise or error now increases as N, $\sigma = N\varepsilon(v)$ and the output signal to noise $SNR_{out} = SNR_{in} = s/e(v)$ which is limited by the differential non-linearity error of the transfer function.

It is obvious that differential non-linearities in any of the amplifiers which are in line before the detection stage will have the same consequences. If an amplifier is operated near the saturation range for a particular frequency component in its bandpass, the differential non-linearity errors may be quite large.

d. Calibration

Calibration of multichannel data serves two purposes, the first is to remove channel by channel variations of gain in the system, and in so doing accomplishes the second which is to establish a physical scale for the measurements. Calibrating an observation can degrade the SNR of the observation. Although this degradation is not an instrumental effect, a detailed examination of the calibration process can show us how to minimize this type of degradation.

Schematically, the output, $S_i$, of each filter channel is given by

$$S_i = G_i \ (T_{sys} + \varepsilon_i \ s_i) \tag{34}$$

where $G_i$ is the channel by channel gain, i = 1 to N where N is the number of channels in a filterbank, $T_{sys}$ is the receiver system temperature, $s_i$ is the signal input to the receiver, and $\varepsilon_i$ represents the frequency response of the receiver front-end. The distinction between $G_i$ and $\varepsilon_i$ is important. Although the $G_i$'s are different channel to channel, they are fairly close in value within the entire IF bandpass; i.e. we choose the RF power amplifiers to have sufficient bandwidth. The front-end response, $\varepsilon_i$, however, may have large variations across the IF bandpass. This is especially true in the 10μm heterodyne receiver (Mumma et al. [10]), where $\varepsilon_i$ falls in sensitivity by a factor of 3 from 0 to 1.6 GHz in the IF. In addition, $\varepsilon_i$ depends strongly on LO power, optical stability, and mixing efficiency. It is important to note that even in the absence of a signal, $s_i$, there will still be an output $S_i = G_i T_{sys}$. Therefore, the front-end gain and time stability can only be sampled if a sufficiently strong signal is present, i.e. $\varepsilon_i$ comes only into play when an input signal, $s_i$, is not zero.

The calibration scheme works the following way. A measurement is taken of a known temperature blackbody, $T_{BB}$, usually chopped with reference to cold sky. Although the sky temperature is 270°K, observations are undertaken where the sky optical depth is relatively small, i.e. where the sky is not opaque. Therefore, it is a good approximation, for our case, to take $T_{sky} = 0$. We get

$$\begin{aligned} S_i &= G_i \ (T_{sys} + \varepsilon_i T_{BB}) \\ R_i &= G_i \ (T_{sys} + \varepsilon_i T_{sky}) \doteq G_i T_{sys} \end{aligned} \tag{35}$$

We take the ratio $(S_i - R_i)/R_i$ channel by channel

$$BB_i = \frac{S_i - R_i}{R_i} = \frac{G_i(T_{sys} + e_i T_{BB}) - G_i T_{sys}}{G_i T_{sys}}$$

$$= \frac{e_i T_{BB}}{T_{sys}} \qquad (36)$$

where $BB_i$ is the blackbody measurement, and $T_{sys}$ is generally not known a priori. $BB_i$ is actually a good measurement of $1/e_i$ which Fig. 7 shows very plainly. A similar ratio is taken with a signal at the receiver input given by $\Delta T_i$. The measurement, $M_i$, is given by

$$M_i = e_i \frac{\Delta T_i}{T_{sys}} \qquad (37)$$

Now we can solve for $\Delta T_i$, using equation (36) since we can scale with the blackbody temperature $T_{BB}$. ($T_{BB}$ is not measured exactly through the same optical path as the signal, i.e. we will ignore telescope or transfer optic efficiencies here.)

$$\Delta T_i = \frac{M_i}{BB_i} T_{BB} \qquad (38)$$

and we have eliminated all gains from the measurement.

Assuming $BB_i$, and $T_{BB}$ are noiseless measurements, the only contribution in uncertainty in measuring $\Delta T_i$ comes from the uncertainty in measuring $M_i$. We can calculate the SNR of a measurement of the type M = (S-R)/R. The noise contribution to M is given by

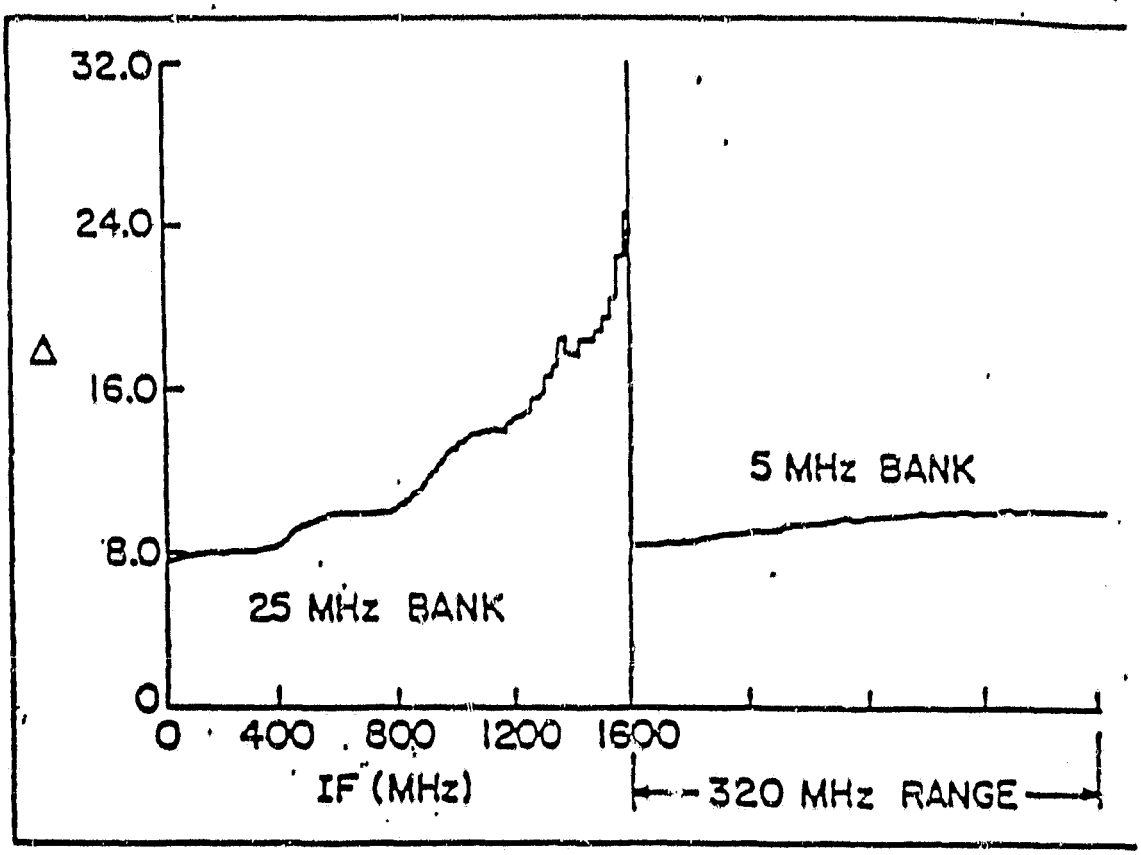


Fig. 7. Measurement of system degradation Δ as a function of IF frequency (0 to 1600 MHz). The three-fold increase in Δ at high IF frequencies is caused by the roll-off of the mixer-preamplifier response.

ORIGINAL PAGE IS
OF POOR QUALITY

$$\sigma_M^2 = \left(\frac{\partial M}{\partial S}\right)^2 \sigma_S^2 + \left(\frac{\partial M}{\partial R}\right)^2 \sigma_R^2$$
$$= \left(\frac{1}{R}\right)^2 \sigma_S^2 + \left(\frac{S}{R^2}\right)^2 \sigma_R^2 \qquad (39)$$

Using $\sigma_S = \sigma_R$ we get

$$\sigma_M = \left(\frac{\sigma}{R}\right)\sqrt{1 + \left(\frac{S}{R}\right)^2} \qquad (40)$$

The signal to noise ratio for M is therefore given by

$$SNR_M = \frac{M}{\sigma_M} = \frac{S-R}{\sigma}\,\frac{1}{\sqrt{1 + (S/R)^2}} = \frac{SNR}{\sqrt{1 + (S/R)^2}} \qquad (41)$$

where we noted that $(S-R)/\sigma$ is the SNR of the signal itself given by equations (19) and (20), the signal to noise ratio has been degraded by

$$\delta = \sqrt{1 + (S/R)^2} \qquad (42)$$

Let $S = \Delta S + R$, where $\Delta S$ is the signal response over the reference. We get from equation (40) that

$$\delta = \sqrt{2 + \left(\frac{\Delta S}{R}\right)^2 + \frac{2\Delta S}{R}} \qquad (41)$$

When $R \gg \Delta S$, then $S = \sqrt{2}$, e.g. $\Delta S = 0$ in a balanced receiver mode; the $\sqrt{2}$ SNR degradation results simply from taking the ratio. For $S/R > 1$, then $\delta \sim S/R$ from equation (40).

It is now easy to see why a Dicke-switched balanced receiver has the highest sensitivity. A balanced receiver operates at the point $S \sim R$, and $\Delta S \ll R$. In absorption observations of atmospheric constituents against the sun or the moon, $\Delta S$ can become a sizable factor with respect to R, especially if the reference is against the sky. To minimize the degradation in SNR of solar absorption spectra, the observations should be chopped against a reference temperature which is greater than or equal to the sun's, i.e. $R \gtrsim \Delta S$, which means $S/R \sim 1$.

## IV. Photodiodes as Square-Law Detectors

In an AOS we must include noise terms which are unique to using photodetectors as total power integrators. These terms are in addition to the sensitivity consideration given in Section III which are common to all total power radiometers. Within the AOS, the photodiodes in a linear array acts as the basic power detectors - they serve the functions of bandpass filters, square law detectors, and power integrators. Since the intensity of diffracted light is proportional to the spectral power of the IF (given by equation 6) at a given frequency, a photodiode, at a particular location, integrates the light and gives an output which is the integrated power at that frequency component. Each output of a pixel in an AOS linear array, therefore, acts as the single channel as shown in the schematic of Fig. 3.

We will discuss here, primarily, a set of commercially available linear arrays of monolithic silicon integrated photodiodes with 1024 elements. Each photodiode is on a 15μm center with dimensions of 7μm width by 16μm (or 300 μm) heights. The diode has an associated storage capacitor on which to integrate photocurrent and a multiplex switch for periodic readout via an integrated shift register scanning circuit. Some properties of a typical diode array (Reticon 1024H) are shown in Fig. 8 [11]. Fig. 8(a) is the detector spectral response, a typical quantum efficiency at the HeNe laser frequency of 632.8 nm is $\eta = 0.7$, a

CW GaAs diode laser operates at $\lambda$ = 850 nm, with $\eta \sim 0.7$. The geometry and aperture response of a pixel is shown in Fig. 8(b). The equivalent circuit of the array is given in Fig. 8(c); notice a row of dummy diodes in parallel to the light sensitive ones.

a) Detector Responsivity and Storage Capacity

The responsity of a photodetector is defined by

$$R_\lambda = \frac{q\eta(\lambda)}{Ahc/\lambda} \qquad \text{(in units of ampere/watt/m}^2 \text{ or coulombs/joule/m}^2\text{)} \tag{44}$$

This number is dependent on the wavelength of light through the quantum efficiency $\eta(\lambda)$, and the photon energy $hc/\lambda$; q is the electronic charge and A is the photoelement exposure area. Typical values for broadband responsivity (over the dotted light source given in Fig. 8(a)) for the Reticon 1024H is R=0.8 $pA/_\mu watt/cm^2$. In order to convert equation (44) to the number of photoelectrons produced by an exposure to light we have

$$n_e(T) = (R_\lambda/q)(hc/_\lambda)(\phi_\lambda AT) \equiv R_{D\lambda}\phi_\lambda T \tag{45}$$

where $\phi_\lambda$ is the flux given by number of photons/sec, and T is the exposure time for the photoelement, and $R_{D\lambda}$ is defined by (45).

Each photoelement has a finite charge capacity which is given by its associated on-chip capacitor. For the Reticon 1024H the storage capacity is Q = 2.2 pcoul which corresponds to a electron capacity of $N_{sat} = 1.37 \times 10^7$ electrons. The maximum integrating time for an array, in the absence of detector noise, is then given by

a) Spectral Response

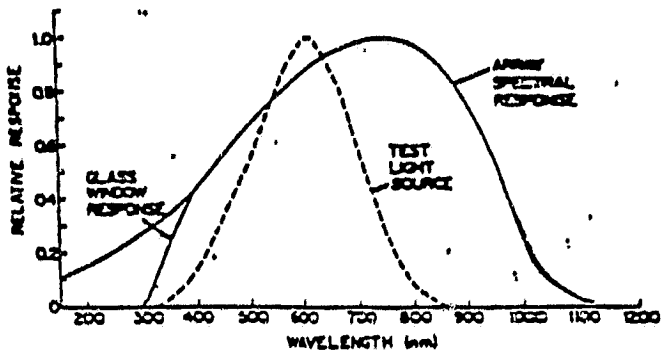


Relative spectral response as a function of wavelength. Dashed line shows spectral distribution of light source used for sensitivity measurements. Quartz and glass windows have similar response except that glass window will fall off at approximately 360 nm as shown above.

b) Pixel Geometry

a= 7 microns

b= 15 microns

c= 16 microns ( or 300 microns)

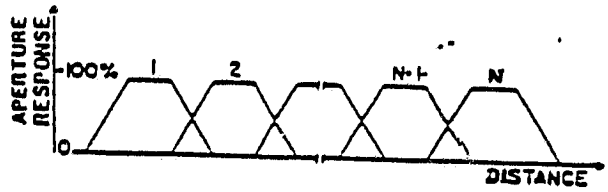


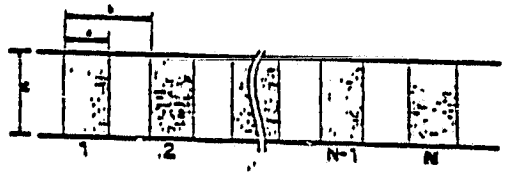


c) Linear Array
equivalent circuit

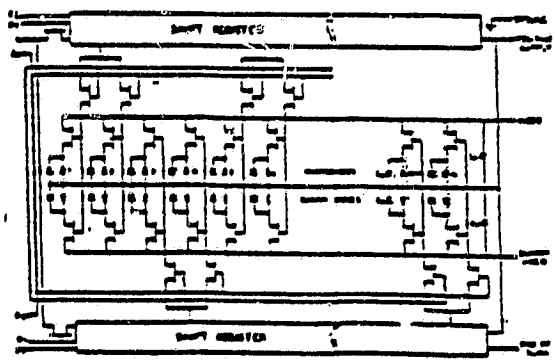

FIGURE 8. Reticon RL1024 H Linear Photo-Diode Array Properties.

$$T \leq N_{sat}/(n\Phi) \tag{46}$$

b) Dark Current and Leakage Current Noise

A photodetector, even in the absence of light, will generate current due to the diffusion of charges generated by thermal excitation. This leakage current will charge up a storage capacitor and, since the generation process is random, contributes temporal noise associated with the sensing of the charge or voltage on the capacitor. The process obeys Poisson statistics and can be described as shot noise. The error given by the process (in units of electrons) is given by

$$Q_n^2 \text{ (leakage)} = qi_L T \tag{47}$$

where $i_L$ is the dark or leakage current and T is the sample time interval. Even in the absence of light, therefore, the leakage current will limit the maximum integration time

$$T_{max} \leq qN_{sat}/i_L \tag{48}$$

For the Reticon 1024H, $i_L$=1.0 pA at room temperature. The leakage current is a very strong function of temperature and will double in value for every 7°C. The dark current contribution will saturate the detector in $T_{max}$ = 2.2 sec at room temperature (25°C).

c) Charge Reset Noise

The noise contribution from the charging of capacitors is important since in a photodetector array this mechanism is used repeatedly to convert a signal from charge to voltage and vice versa (see Borsuk [12]). Within a detector a capacitor whose initial charge is zero is to be charged to a voltage $V_o$, through

a resistor R by closing a noiseless switch. The voltage across the capacitor is then given by

$$V(t) = V_o\ (1 - e^{-t/RC}) \tag{49}$$

or in terms of the charge

$$Q(t) = CV_o\ (1 - e^{-t/RC}) \tag{50}$$

The variance on the mean value of Q(t) has been shown by Barbe [13] to be given by equation (51) where T is the temperature and k is Boltzmann's constant;

$$\bar{Q}(t)^2 = kTC\ (1 - e^{-2t/RC}) \tag{51}$$

The signal detection process involves two steps. The first is the fast charging up of the capacitor by the action of a low resistance switch. The second comes from the discharging of the capacitance by photogenerated charges when the switch is turned off. As noted before, thermally generated leakage current also contribute to this process and adds shot noise. The RC/2 time constant associated with equation (51) is different for the two processes. In the charging mode a typical MOS switch, which has a nominal value of $R = 10^4\Omega$ charging up to 2.2 pcoul, has a time constant $RC/2 = (10^4\Omega \times 0.2pF)/2 = 1$ nsec. When the switch is turned off, then $R \doteq 10^{12}\Omega$, and $RC/2 = 0.1$ sec. Consequently, after $t = 5RC$ in the charge mode the mean deviation is given by

$$Q_n = (kTC)^{1/2} \tag{52}$$

If we sample the charge immediately after the low resistance switch has been turned off, we can then get a measurement of $Q_n$ without any additional noise since the time constant is so long. This noise contribution can be taken out by subtracting it from the measurement after an exposure time t.

This type of signal processing is commonly called correlated double sampling (CDS), and is used to subtract out the charge reset noise. We can calculate the noise equivalent electron number given by equation (52) since $N_e = \bar{Q}_n/q = \sqrt{kTC}/q$. In terms of C given in pF and $T = 300^oK$ we get

$$N_e = 400\sqrt{C} \tag{53}$$

The detector storage capacitance on the Reticon 1024H is given by $C = Q_{sat}/V_o$ where Vo is the charging voltage. $Q_{sat}$ = 2.2 pCoul and $V_o$ = 12V, therefore $C = 2.2 \times 10^{-12}/12 = 0.18$ pF. The noise equivalent electrons is then given by equation (53) $N_e = 400\sqrt{0.18} = 171$ electrons. However, each detector is then read out of a common video line which has a 35 pF capacitance. This readout noise is, $N_{readout} = 400\sqrt{35} = 2336$ electrons. Therefore, the mean noise is dominated by video readout noise. It must be noted that the charge reset noise is a post-detection factor which will occur at the same level after the sampling of each detector element, and is therefore independent of the exposure time.

d. Signal and Background Shot Noise

Whenever discrete particles arrive at random times, there will be fluctuations in the rate of arrival. The detection of light involves the measurement of the arrival of photons, and therefore the fluctuations in the rate of arrival constitutes an additional noise source which is called shot noise. This type of process can be analysed in a straight forward way (see Oliver [14]) and we will briefly derive the result. We assume that a photon is equally likely to arrive at any time but that it arrives at an average rate, r. This means that if we measure n photons arriving within a time t, the limit as t

$\to \infty$ of $n/t \to r$. In a time interval $\Delta t \ll 1/r$, the probability of detecting a photon is just $r\Delta t$ and the probability of <u>not</u> detecting a photon is $(1-r\Delta t)$. Therefore the probability of <u>no</u> arrivals during t is given by

$$p_0(t) = \lim_{\Delta t \to 0} (1-r\Delta t)^{t/\Delta t} \tag{54}$$

since there are $t/\Delta t$ independent intervals during which no arrival must occur, and taking the limit, equation (54) becomes

$$p_0(t) = e^{-rt} \tag{55}$$

The probability of exactly one arrival in time t is the probability of receiving a particle in the interval $\tau$ to $\tau+d\tau$ and none before or after, summed over all $\tau$. We then have

$$p_1(t) = \int_0^t p_0(t)\ [r d\tau]\ p_0(t-\tau)$$

$$= rt\ e^{-rt} \tag{56}$$

For the arrival of two photons, the probability is given by one arrival before $\tau$, one arrival in the interval $\tau+d\tau$, and none after, i.e.

$$p_2(t) = \int_0^t p_1(\tau)\ [r d\tau]\ p_0(t-\tau)$$

$$= \frac{(rt)^2}{2!}\ e^{-rt} \tag{57}$$

And in general for n arrivals we get

$$p_n(t) = \frac{(rt)^n}{n!} e^{-rt} \tag{58}$$

The mean value of n, is given by

$$\bar{n} = \Sigma\, n\, p_n(t) = rt \tag{59}$$

from evaluating equation (58) and (59), as it should be from the definition of rt. We can obtain a recursive definition for $p_n(t)$ from equation (59) and get

$$p(n) = \frac{(\bar{n})^n}{n!} e^{\bar{n}} = \frac{\bar{n}}{n} p(n-1) \tag{60}$$

The deviation from the mean is derived from

$$(\delta n)^2 = \Sigma\, p(n)\, (n-\bar{n})^2$$

$$= n^2 - (\bar{n})^2 \tag{61}$$

and we can calculate

$$\bar{n}^2 = \Sigma\, n^2\, p(n) = \bar{n} + (\bar{n})^2. \tag{62}$$

Therefore we get the simple result that

$$(\delta n)^2 = \bar{n} \text{ or } \delta n = \sqrt{\bar{n}} \tag{63}$$

In an AOS, the diffracted light level detected by the photodetector array will be a large constant, due to the receiver noise, plus a small contribution due to the signal. In addition a contribution due to scattered ambient light from the laser can be present. If we represent the photon flux from the receiver noise plus signal as $\Phi_S$ and the background term as $\Phi_B$, then the detector output is given by equation (45), and the noise contribution will be given by

$$(\delta n)^2 = R_{D\lambda} \quad (\Phi_S + \Phi_B)T \tag{64}$$

Careful optical arrangement can minimize $\Phi_B$, but the contribution from the signal term will always be present.

If we operate near saturation $n_e = 1 \times 10^7$ electrons, then the dynamic range is limited by the signal shot noise as given by $n_e/\sqrt{n_e} = 3 \times 10^3$ or 30 dB. We see that $\delta n_e = 3 \times 10^3$ electrons, and this value is comparable to the charge reset noise of $\sim 2 \times 10^3$ electrons derived in the previous section.

c) Laser Stability and Mechanical Alignment

Two potential sources of receiver fluctuation inherent in an AOS is the stability and added noise of the laser light source. In a bulk Bragg cell system a HeNe laser is used as the coherent light source. Since the optical components are made up of discrete parts, overall mechanical stability of the system must also be considered. In an integrated optics AOS, the laser light source is a solid state GaAlAs diode laser which is precisely butt-coupled to one end of $LiNbO_3$ substrate on which lenses and transducers are fabricated. Mechanical alignment and jitter have been minimized by the compact and structurally integral package. However diode lasers may be susceptible to ion plasma noise.

The fluctuations in power of the Spectra Physics Model 120 HeNe laser, which we use in our bulk Bragg cell AOS, is specified to be <0.5% from 1-100

kHz, and amplitude ripple is less than <0.2% up to 120 Hz. The primary cause of amplitude noise in the HeNe laser is intermodulation of the optical frequencies, primarily five optical resonant frequencies spaced about 300 MHz apart within the 1500 MHz half-width temperature-broadened neon gain profile. When the resonant frequencies are combined in a non-linear detector, as in a photodiode, the output contains all possible difference frequencies between the optical frequencies present. These intermodulation products appear noise-like since the frequency components vary rapidly with small cavity changes. The intermodulation products limit the minimum noise level in the 1 KHz to 100 KHz range of the HeNe laser.

A photodiode in addition to acting as a square-law detector is also an integrating element, and therefore acts as a low pass filter. For an integration time in a photodetector of ~10 msec, the detector filters out fluctuations above 50 Hz (the Nyquist frequency). Fluctuation of the 5 mW laser at this frequency has been specified at 0.2%. Noise sources at these frequencies can be treated as gain fluctuations as described previously at in section IIIa, and can be minimized by Dicke-switching.

In a bulk Bragg cell AOS system, the primary consequence of mechanical jitter is the frequency stability of the spectrometer caused by errors in the optical pointing. Proper mechanical design and rigid mounting of optical parts can minimize this problem. Measurements of frequency error in a prototype AOS system has shown that optical alignment can be attained to within a detector pixel, about 10$\mu$m. Fig. 9 shows the frequency stability of a single tone observed on an AOS over a timescale of over 3 hours. The ordinate scale represents channel number or position of a single pixel.

A potential source of error in using an AOS for detecting signals which are as narrow as the frequency resolution of an AOS is an effect called "scalloping loss." This effect results from the fact that output plane of the Bragg cell is sampled only at discrete positions with an aperture resolution which does not totally overlap neighboring detectors (see Fig. 8), i.e. if a narrowband frequency component happens to fall between two detectors, the resulting amplitude output will be divided between the two pixel elements. In this case a measurement of the strength of the signal will be seriously underestimated.

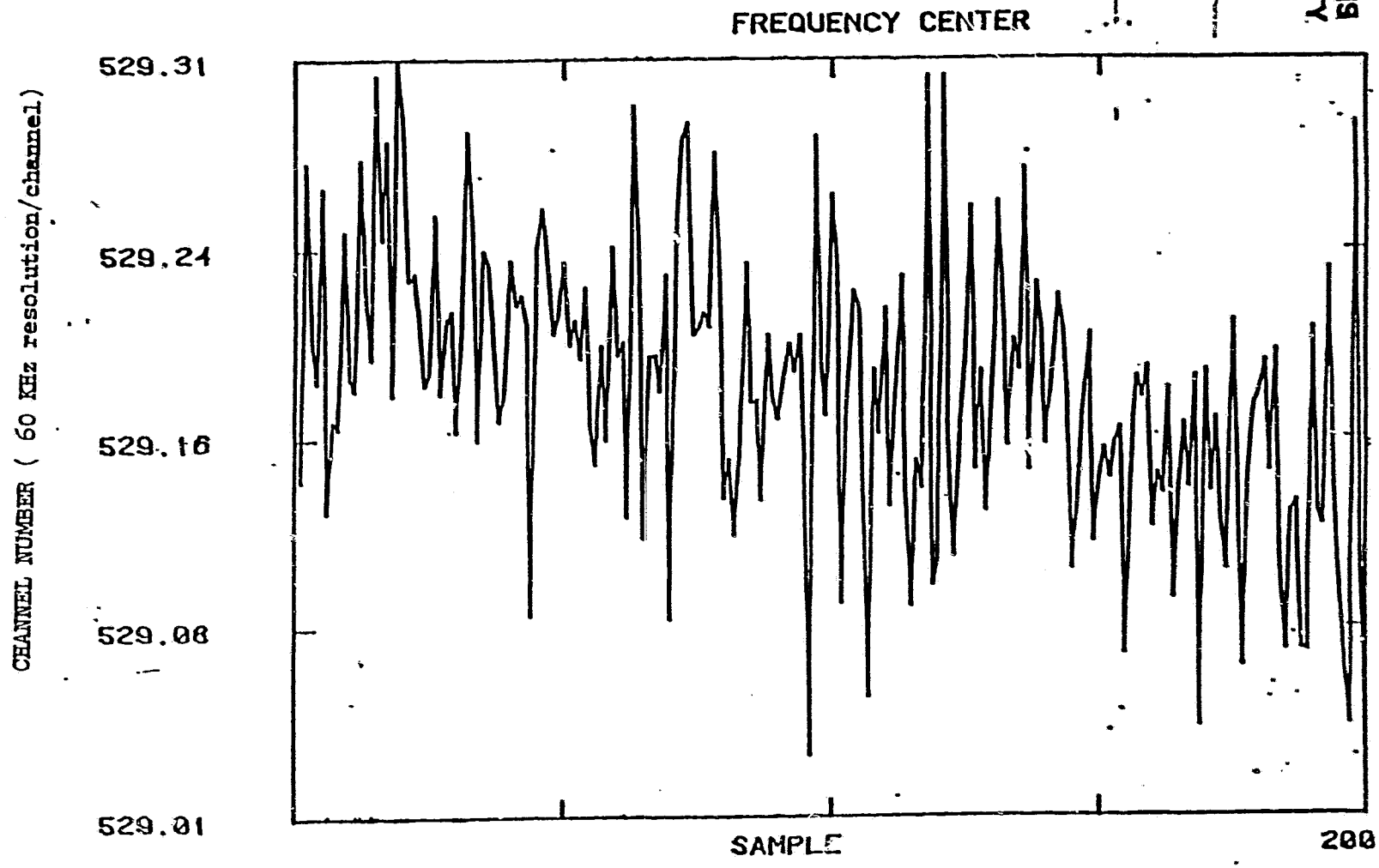


FIGURE 9. Frequency or mechanical stability of an AOS.
Each sample corresponds to 1 minute interval.

This problem is entirely analogous to the use of digital FFT's to estimate spectral components when the number of points in the FFT is not large enough to sample the narrowest frequency component. This effect is usually not a serious one in astronomical applications, since spectral features are often much wider than a single resolution element.

## V. Summary of Noise Terms

We see in section II that an improvement in SNR from the original input SNR can be obtained by both analog and digital processing. This is an essential feature since the input SNR can be as low as $10^{-3}$ or $10^{-4}$ with submillimeter heterodyne receivers now being used or under development. However, degradations to this processing gain comes from several sources; some outlined in section III are common to all total power radiometers, and others as outlined in section IV, are uniquely attributed to the AOS which depends on photodetectors and a coherent light source as the detection system. We rewrite equation (22) with the degradation term denoted by $\delta$.

$$SNR_{out} = \frac{\sqrt{JBT}}{2} \frac{SNR_{in}}{\delta} \tag{65}$$

where BT is the time bandwidth factor, and J comes from the number of digital samples. T is limited in an AOS by several factors, primarily by the saturation capacity of a photoelement. J, however, is only limited by the digital precision in which the digital processing takes place. The degradation can be written as

$$\delta^2 = 1 + \sum_{i}^{N} \delta_i^2 \tag{66}$$

where we denoted the extra noise contributions by $\delta_i^2$, which we summarize below.

1) Gain Instability as described in section IIIa and which may include laser and mechanical stability described in section IVe. This term is given by

$$\delta_1^2 = (\Delta F')^2 / BT \tag{67}$$

where $\Delta F'$ percentage of $\sigma_{RF}$ gain noise present even after Dicke-switch filtering.

2) ADC Quantization Noise

$$\delta_2^2 = K^2/12BT \tag{68}$$

where $K<1$ and K is the scale factor of the quantization step with respect to the RF noise, i.e. $\Delta = K\sigma_{RF}$. This term can be ignored in a properly operating system. For example $K = 1$ using the worse case, $B = 1$ MHz, $T = 1 \times 10^{-3}$ sec, then $BT = 10^3$, which means $\delta_2^2 = 8 \times 10^{-5}$

3) Diode Leakage Current

$$\delta_3^2 = i_L/(\sigma_{RF}^2 B) \tag{69}$$

4) Diode Charge Reset Noi

$$\delta_4^2 = \frac{KTC}{q^2\sigma_{RF}^2 Bt} = \frac{16 \times 10^4\ C}{\sigma_{RF}^2 Bt} \tag{70}$$

where C is measured in pF, and where t is now the integration time, and T is the temperature.

5) Signal and Background Shot Noise

$$\sigma_5^2 = R_{D_\lambda} \frac{\phi_{S+O_B}}{\sigma^2_{RF} B} \tag{71}$$

The above five terms are uncorrelated noise terms which do not alter the fact that the processing gain increases as $\sqrt{JBT}$ given by equation (65). However, we also pointed out in section IIId, that the errors associated with differential non-linearities, are correlated with one another, and therefore cannot be processed out. The processing gain may be limited by

$$SNR_{out} \lesssim \frac{S}{\epsilon(v)} \tag{72}$$

where $S/\epsilon(v)$ is the SNR determined by the differential non-linearity at a particular operating point.

Finally, we have a degradation in SNR due to the arithmetic processing of the observed data in order to cancel channel to channel gain variations. Although this effect is not instrumental in nature its analysis enables us to minimize this factor by reconsidering our observing scheme. This degradation is discussed in section IIIe, and is an additional term which must degrade equation (61).

$$SNR_{Process} = \frac{SNR_{out}}{\delta_{Process}} \tag{73}$$

where

$$\delta^2_{process} = 1 + (S/R)^2 \tag{74}$$

where S is a measurement of a signal and R is a measurement of a reference load in a Dicke switch system.

References

[1] T. R. Ranganath, T. R. Joseph, and J. Y. Lee, "Integrated Optical Circuits for RF Spectrum Analysis," Technical Report Hughes Research Laboratories, AFWAL-TR-80-1004, Avionics Laboratory Air Force Systems Command, Wright-Patterson AFB, OH 45433.

[2] E. H. Young, Jr., S. K. Yao, "Design Considerations for Acousto-Optic Devices," Proceedings of the IEEE, Vol. 69, No. 1, January 1981, pp 54-64.

[3] A. Korpel, "Acousto-Optics - A Review of Fundamentals," Proceedings of the IEEE, Vol. 69, No. 1, January 1981, pp 48-53.

[4] J. D. Kraus, "Radio Astronomy", chapter on Radio-Telescope receivers by M. E. Tiuri, McGraw-Hill Books, 1966, pp 236-293.

[5] W. J. Lucas, "Tangential sensitivity of a detector video system with r.f. preamplification," Proc. IEE (London), Vol. 113, No. 8, August 1966, pp 1321-1330.

[6] P. Kellmar, H. N. Saver, J. W. Murray, "Integrating Acousto-Optic Channelized Receivers," Proceeding of the IEEE, vol. 69, No. 1, January 1981, pp 93-100.

[7] T. M. Turpin, "Time Integrating Optical Processors," Proceedings of SPIE, Real Time Signal Processing, Vol. 154, 1978, pp 196-203.

[8] A. D. Whalen, "Detection of Signals in Noise," Academic Press, New York, 1971, pp 99-118.

[9] R. H. Dicke, "The Measurement of Thermal Radiation at Microwave Frequencies," Rev. Sci. Instr., Vol. 17, July 1946, pp 268-275.

[10] M. J. Mumma, T. Kostiuk, D. Buhl, D. Deming, G. Chin, "Infrared Heterodyne Spectroscopy," Optical Engineering, Vol. 21, No. 2, March-April 1982, pp 313-319.

[11] EG&G Reticon Data sheet on H-series Solid State line scanners 1024, 1728, and 2048 elements.

[12] G. M. Borsuk, "Photodetectors for Acousto-Optic Signal Processors", Proceedings of the IEEE, Vol. 69, No. 1, January 1981, pp 100-118.

[13] D. F. Barbe, "Imaging devices using the charge-coupled concept," Proceedings of the IEEE, vol. 63, January 1975, pp 38-67.

[14] B. M. Oliver, "Thermal and Quantum Noise", Proceedings of the IEEE, vol. 53, May 1965, pp 436-454.